

# Source Exploration for an Under-Actuated System: A Control-Theoretic Paradigm

Xiangyuan Jiang<sup>ID</sup>, Shuai Li<sup>ID</sup>, Senior Member, IEEE, Bing Luo,  
and Qinghao Meng, Member, IEEE

**Abstract**—The task of seeking an unknown source with the measurements of the emitted signal strength is named as the source-exploration problem, whose challenging issues with conducting autonomous source-exploration are the lack of *a priori* knowledge about the distribution of the emitted signal and the presence of unignorable noise in both the propagation situation and equipped sensor readings. This paper presents a planner for an autonomous robot engaged in seeking for an odor source. The guidance strategy for the planner is based on a control-theoretic paradigm which incorporates an optimization technique into the structure. The control law is inspired by two prominent behaviors widely observed in biology, namely, chemotaxis and anemotaxis. The two behaviors are formulated in the control development. The derived control law is rigorously analyzed and guarantees the converge of a nonlinear under-actuated robot to reach the unknown source, which provides a case study on using run-time optimization to guide rigorous control algorithm development. Besides theoretical proof, our results are also validated in numerical simulations and physical experiments.

**Index Terms**—Optimization algorithm, source exploration, under-actuated systems.

## I. INTRODUCTION

SOURCE seeking aims to locate an unknown source by moving toward it without any attempt to estimate other parameters such as the release rate [1], which is useful in many military and industrial applications, i.e., explosive detection, drug detection, and pollution sensing.

Underactuated plants, i.e., surface vessels [2], aircrafts [3] and vehicles, are kinds of typical systems used for source seeking. The investigations on how to deploy underactuated agents in chemical leakage fields are meaningful in both

Manuscript received December 2, 2018; accepted January 26, 2019. Date of publication March 1, 2019; date of current version April 13, 2020. Manuscript received in final form January 30, 2019. This work was supported in part by the National Natural Science Foundation of China under Grant 61503413, Grant 61573253, Grant 6161101383, and Grant 61711530133, in part by the Hong Kong Research Grants Council Early Career Scheme under Grant 25214015, in part by the Departmental General Research Fund of Hong Kong Polytechnic University under Grant G.61.37.UA7L, and in part by PolyU Central Research Grant under Grant G-YBMU. Recommended by Associate Editor W. He. (*Corresponding author: Shuai Li*)

X. Jiang is with the Institute of Marine Science and Technology, Shandong University, Qingdao 251007, China, and also with the Department of Computing, The Hong Kong Polytechnic University, Hong Kong (e-mail: shiangjuan@gmail.com).

S. Li is with the Department of Computing, The Hong Kong Polytechnic University, Hong Kong (e-mail: shuaili@polyu.edu.hk).

B. Luo and Q. Meng are with the School of Electrical and Information Engineering, Tianjin University, Tianjin 307459, China (e-mail: bluo@tju.edu.cn; qh\_meng@tju.edu.cn).

Color versions of one or more of the figures in this article are available online at <http://ieeexplore.ieee.org>.

Digital Object Identifier 10.1109/TCST.2019.2897504

practice and theory to find the leakage source point. Control-based method depending on the model of differential equation usually gathers a plenty of prior information, and shows great performance on source seeking for the under-actuated system.

An amount of investigation has been carried out on source exploration with autonomous robots based on the idea of bio-inspiration [4]–[7]. Russell *et al.* [4] investigated some chemotaxis algorithms inspired by the bacterium, the silk-worm moth, the dung beetle, as well as a gradient-based algorithm. Compared to the chemotaxis algorithms relying on local concentration gradients, Vergassola *et al.* [5] proposed an “infotaxis” strategy by maximizing the expected rate of information gain instead of the gradient. Masson *et al.* [6] extended the “infotaxis” to find sources of particles and designed decision-making strategies by maximizing the rate of acquisition of information on the location of the source which could balance the exploration and exploitation. Similarly, Hajieghrary *et al.* [7] presented a multiagent collaborative “infotaxis” strategy based on the general structure of [5], which used the relative entropy to generate a search strategy for multiagent systems.

Optimization and Bayesian methods introduced probabilistic robotics to the source localization problem [8]–[10]. Zou *et al.* [8] proposed a planner for a swarm of robots engaged in seeking an electromagnetic source based on particle swarm optimization which was a bio-inspired optimization technique. Pang and Farrell [9] presented a source-likelihood mapping approach with Bayesian inference methods to locate the source of the chemical plume using an autonomous vehicle, which was capable of detecting the chemical concentration and sensing the flow velocity. Li *et al.* [10] designed an odor source localization algorithm, using a robot performing both exploratory and exploiting behaviors, based on particle filters in an outdoor airflow environment.

The advantages of control algorithm attract many researchers to study them and apply them to the source seeking problem [11]–[15]. Cochran *et al.* [11] developed control laws by using extremum seeking along a predetermined path for an underwater vehicle which is similar to the way a fish moves. Furthermore, they extended the relevant results to three-dimensions situation [12] introducing challenges such as the choice of the vehicle model, sensor placement, and the pattern of under-actuated motion. Finally, they presented two control schemes: one focused on vehicles with a constant forward velocity, the other one employed vehicles with constant forward and pitch velocities. Fu and Ozguner [13] proposed a source-tracing algorithm utilizing extremum-seeking control

with sliding mode to find direction and using variable structure control to address the constraints on vehicle kinematics and the access area. Raisch and Krstic [14] presented a composite control law to achieve good qualities on transient and asymptotic performances, which was efficient in approaching to the source and hovering around the source. The trajectories generated by extremum seeking always demanded costly maneuvers. Li *et al.* [15] proposed a source seeking algorithm by using a robot team cooperatively to estimate the gradient of the source field, move to the source by tracing the gradient-ascending direction, and keep a predefined formation in movement.

Specifically, we successively consider the control structure for source seeking using a robot. An observer-based controller accompanying with position feedback under kinematic model is formulated in a single integral form. And then, the heading of the robot is adopted as another variable in the control structure and attitude control problem is converted to feedback linearization problem for the under-actuated system.

This paper is structured as follows. Source seeking problem is formulated in Section II. In Section III, a novel controller is proposed to solve the problem, and the optimization is further designed for the controller. In Section IV, theoretical analyses are presented. In Section V, simulations and experiments are conducted. In Section VI, the conclusion is drawn. Before the end of the introduction, it is worth pointing out that remarkable points of this paper mainly lie in three aspects.

- 1) Two prominent classes of algorithms exist in the field of source exploration, i.e., behavior-based algorithms and control oriented algorithms. However, there is a clear gap between them. This is the first source exploration algorithm that starts from bio-inspiration (chemotaxis and anemotaxis) but bears a solid theoretical foundation with provable convergence and stability.
- 2) This work addresses three tasks, i.e., nonactuated system control, upstream moving, and signal strength maximization, in a unified control framework for source seeking.
- 3) In terms of control and optimization, the theoretical analysis on convergence and stability are conducted to guarantee the performance of the proposed structure.

## II. PRELIMINARIES

In this section, we present models and assumptions on robot and environment, and illustrate the source seeking problem.

### A. Source Propagation Model

The propagation model of contaminant is modeled by advection-diffusion equation [16]

$$\frac{\partial c}{\partial t} - \mathbf{v}^T \nabla c = k_0 \nabla^2 c \quad (1)$$

where  $\{c \geq 0 | c \in \mathbb{R}^1\}$ , relative to space variable  $\mathbf{x}$  and time variable  $t$ , represents the scalar field of contaminant.  $\partial c / \partial t$  denotes the partial derivative of  $c$  along  $t$ ,  $\mathbf{v}$  is the advection velocity,  $k_0$  is the diffusion coefficient,  $\nabla c \in \mathbb{R}^2$  is the spatial gradient of  $c$ , and  $\nabla^2 c \in \mathbb{R}^1$  is the divergence of  $c$ .

Source propagates according to (1), and then, following the reverse-propagation direction, the concentration  $c$  at the mass

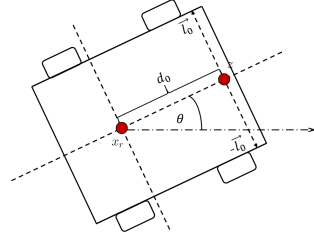


Fig. 1. Sketch of the robot used for source seeking.

point of a robot used for source seeking at point  $\mathbf{x}_s$  satisfies

$$\dot{c} = -\frac{\mathbf{v}^T \nabla c + k_0 \nabla^2 c}{\|\nabla c\|^2} \quad (2)$$

### B. Kinematic Model of the Robot

For a robot used for source seeking, its mass point  $\mathbf{x}_r = [x_{r1}, x_{r2}]^T$  in the global coordination and heading angle  $\theta$  could be formulated as [17], [18]

$$\begin{bmatrix} \dot{x}_{r1} \\ \dot{x}_{r2} \\ \dot{\theta} \end{bmatrix} = \begin{bmatrix} \cos \theta & 0 \\ \sin \theta & 0 \\ 0 & 1 \end{bmatrix} \begin{bmatrix} w_1 \\ w_2 \end{bmatrix} \quad (3)$$

where  $\mathbf{w} = [w_1, w_2]^T$  denotes the translational speed and the rotational speed, respectively, defined in the local coordination.

### C. Dynamic Model of the Robot

The dependence of  $\mathbf{w}$  on the thrust force  $\mathbf{h} = [h_1, h_2]^T$  is constituted as follows [19]:

$$\begin{aligned} \dot{w}_1 &= -\alpha_1 w_1 - \beta_1 (h_1 + h_2) \\ \dot{w}_2 &= -\alpha_2 w_2 + \beta_2 (h_2 - h_1) \end{aligned} \quad (4)$$

where  $\alpha_1$ ,  $\alpha_2$ ,  $\beta_1$ , and  $\beta_2$  are all positive constants. Define

$$A = \begin{bmatrix} -\alpha_1 & 0 \\ 0 & -\alpha_2 \end{bmatrix}, \quad B = \begin{bmatrix} -\beta_1 & -\beta_1 \\ -\beta_2 & \beta_2 \end{bmatrix}$$

where  $A$  and  $B$  are two invertible constant matrices. Then the dynamic model (4) changes to the following:

$$\dot{\mathbf{w}} = A\mathbf{w} + B\mathbf{h}. \quad (5)$$

The simplest way of underactuation situations occurs when the system has a lower number of control inputs than degrees of freedom. For the robot system consisting of both the kinematic model (3) and the dynamic model (5), there exist two scalar inputs (i.e.,  $h_1$  and  $h_2$ ), while three scalar output (i.e.,  $x_1$ ,  $x_2$ , and  $\theta$ ), which is called an under-actuated system. In term of the under-actuated system, a reference point  $\mathbf{z} = [z_1, z_2]^T$ , instead of the mass point  $\mathbf{x}_r$ , is usually used to solve the attitude control problem by feedback linearization. It is worth pointing out that  $z_1$  and  $z_2$  represent the coordination of the reference point along  $x$ -axis and  $y$ -axis in global framework, respectively, and the reference point is usually selected randomly in front of the mass point [20].

*Problem:* Consider the seeking behavior of the mass point  $\mathbf{x}_r$  of the robot patrolling around the source point  $\mathbf{x}_s$  and

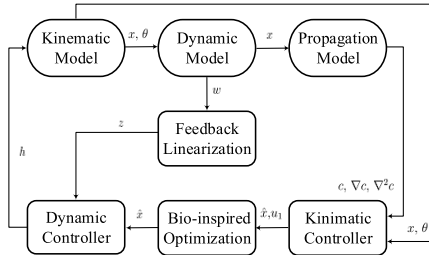


Fig. 2. Control block diagram of the single robot used for source seeking.

the coming assumptions about the robot and the environment as shown in Figs. 1 and 2.

- 1) Suppose there are two sensors mounted on both sides of  $\mathbf{x}_r$  symmetrically, which are located at  $\mathbf{x}_1$  and  $\mathbf{x}_2$  and are  $2l_0$  away from each other. When the robot is moving, both sensors could measure the concentration  $c_1$  and  $c_2$ , respectively, in real time.
- 2) Suppose the reference point  $\mathbf{z}$ ,  $d_0$  away from the mass point  $\mathbf{x}_r$ , incorporates  $\mathbf{x}_r$  to designate the heading direction of the robot and could be developed to demonstrate the kinematic state of the robot sufficiently.
- 3) Suppose the robot's onboard sensors could obtain measurements of mass position  $\mathbf{x}_r$ , heading angle  $\theta$  and environment information at its position such as concentration  $c_r$ , and wind velocity  $\mathbf{v}$ , when it seeks the source following the propagation model (2) at a desired speed  $\mathbf{v}_d$ . It makes sense of that, the robot could get its attitude and position at each time sample, and could measure the concentration and wind velocity at the same time.

Given the source concentration  $c_s$ , design a single integral control  $\mathbf{u}_1$  with position feedback and a dynamic control  $\mathbf{u}_2$  with feedback linearization so that the robot converges to the source point with value  $c_s$  in the constraint of bounded measurements  $c_1$  and  $c_2$ . That is to say, as  $t \rightarrow \infty$ , the objective would achieve  $\mathbf{x}_r \rightarrow \mathbf{x}_s$ .

### III. CONTROL DESIGN

In this section, to deal with the source seeking problem mentioned above, an observer-based control structure [21] is presented in the constraint of kinematic model (2) with a position feedback. Furthermore, to realize the searching strategy, the proposed control structure introduces a novel under-actuated dynamic model using feedback linearization method to figure out the behavior of the robot clearly. In the latter, projection is used to optimize the estimation of the proposed observer based on the inspiration of beetle's foraging with a pair of long antennae.

#### A. Control Design at Kinematic Level

During the process of source seeking, the robot moves back to the source following the reverse-propagation model (2), and at the same time patrols along the tangent direction of the source propagation at speed  $v_d$ . Hence, we could formulate

the following state equation:

$$\dot{\mathbf{x}} = -\frac{(\mathbf{v}^T \nabla c + k_0 \nabla^2 c) \nabla c}{\|\nabla c\|^2} - \frac{\mathbf{v}_d G \nabla c}{\|\nabla c\|} \quad (6)$$

where  $\mathbf{x}$  denotes the reference point of the source seeking, symbol  $\dot{\mathbf{x}}$  is the derivative of  $\mathbf{x}$ , i.e.,  $\dot{\mathbf{x}} = d\mathbf{x}/dt$ , consisting of two terms. The first term in the right part of (6) represents the motion velocity of robot in the inverse direction of propagation, and the second term represents the perpendicular direction of the contour with the maximum motion velocity  $v_d$ . The parameter  $G$  is an orthogonal matrix, in details, which could be written as

$$G = \begin{bmatrix} \cos\theta & \sin\theta \\ \sin\theta & -\cos\theta \end{bmatrix}.$$

The measurement  $c(x)$  is obtained by the sensor equipped on the robot locating at the mass point  $\mathbf{x}_r$ .

Then, we could formulate the measurement equation by using the first-order Taylor expansion

$$y(\mathbf{x}) = \nabla^T c_r (\mathbf{x} - \mathbf{x}_r) + c_r \quad (7)$$

where  $y(\mathbf{x})$  denotes the measurements at time  $t$  obtained by the robot at location point  $\mathbf{x}$ ,  $\nabla^T c_r$  is the gradient of concentration  $c_r$  at point  $\mathbf{x}_r$ . Assume when the mass point  $\mathbf{x}_r$  reaches the source point, the measurement satisfies  $y(\mathbf{x}) = c_s$ .

For the system [22] consisting of (6) and (7), we design a Luenberger-like observer to estimate the state

$$\hat{\dot{\mathbf{x}}} = -\frac{(\mathbf{v}^T \nabla c_{\hat{\mathbf{x}}} - k_0 \nabla^2 c_{\hat{\mathbf{x}}}) \nabla c_{\hat{\mathbf{x}}}}{\|\nabla c_{\hat{\mathbf{x}}}\|^2} - k_1 \frac{\mathbf{v}_d G \nabla c_{\hat{\mathbf{x}}}}{\|\nabla c_{\hat{\mathbf{x}}}\|} - k_2 \nabla c_{\hat{\mathbf{x}}} (\nabla^T c_{\hat{\mathbf{x}}} (\mathbf{x}_r - \hat{\mathbf{x}}) + c - c_s) \quad (8)$$

where  $\hat{\mathbf{x}}$  represents the estimation of  $\mathbf{x}$  to approximate the state of a point on plume front,  $k_1$  and  $k_2$  are coefficients. Unfortunately, the quantities  $c_{\hat{\mathbf{x}}}$ ,  $\nabla c_{\hat{\mathbf{x}}}$ , and  $\nabla^2 c_{\hat{\mathbf{x}}}$  are unmeasurable at the position  $\mathbf{x}$ , for which the quantities at position  $\mathbf{x}_r$  are substitute. Then, the observer (8) could be further rewritten as

$$\dot{\hat{\mathbf{x}}} = -\frac{(\mathbf{v}^T \nabla c_{\mathbf{x}_r} - k_0 \nabla^2 c_{\mathbf{x}_r}) \nabla c_{\mathbf{x}_r}}{\|\nabla c_{\mathbf{x}_r}\|^2} - k_1 \frac{\mathbf{v}_d G \nabla c_{\mathbf{x}_r}}{\|\nabla c_{\mathbf{x}_r}\|} - k_2 \nabla c_{\mathbf{x}_r} (\nabla^T c_{\mathbf{x}_r} (\mathbf{x}_r - \hat{\mathbf{x}}) + c - c_s). \quad (9)$$

For the kinematic model (3) which could be converted into a single integrator model by defining a new controller  $\mathbf{u}_1$ , we propose the following feedback controller, which is definitely distinct from the structures in [23]–[25], to reduce the kinematic model to a single integral model  $\dot{\mathbf{x}}_r = \mathbf{u}_1$

$$\mathbf{u}_1 = -\frac{(\mathbf{v}^T \nabla c_{\mathbf{x}_r} - k_0 \nabla^2 c_{\mathbf{x}_r}) \nabla c_{\mathbf{x}_r}}{\|\nabla c_{\mathbf{x}_r}\|^2} - k_1 \frac{\mathbf{v}_d G \nabla c_{\mathbf{x}_r}}{\|\nabla c_{\mathbf{x}_r}\|} - k_2 \nabla c_{\mathbf{x}_r} (\nabla^T c_{\mathbf{x}_r} (\mathbf{x}_r - \hat{\mathbf{x}}) + c - c_s) - k_3 (\mathbf{x}_r - \hat{\mathbf{x}}) \quad (10)$$

where  $k_3$  is a coefficient for users to select.

#### B. Control Redesign at Dynamic Level

For our application, we mainly care about the position control of the robot. In control-base structure (10) for source seeking mentioned above, the robot has single integrator dynamics of the position and the goal of this section is to

obtain the heading of the robot and to design feedback control such that the robot dynamics converge to a single integrator dynamic control law written as  $\dot{z} = f(z)$ , where  $z$  is the reference point of the robot defined according to assumption (2)

$$\dot{z} = \begin{bmatrix} x_{r1} + d_0 \cos\phi \\ x_{r2} + d_0 \sin\phi \end{bmatrix}. \quad (11)$$

Calculating its derivative yields  $\dot{z} = v = Cw$ , where  $w$  denotes the translational and rotational speeds, and the matrix  $C$  and its inverse  $D$  are defined as

$$C = \begin{bmatrix} \cos\phi & -d_0 \sin\phi \\ \sin\phi & d_0 \cos\phi \end{bmatrix}, \quad D = \begin{bmatrix} c \cos\phi & \sin\phi \\ -\sin\phi/d_0 & \cos\phi/d_0 \end{bmatrix}.$$

According to  $\dot{z} = v$  and model (3), we obtain

$$\dot{v} = \dot{C}w + CAw + CBh \quad (12)$$

where

$$\dot{C} = w_2 \begin{bmatrix} -\sin\phi & -l_0 \cos\phi \\ \cos\phi & l_0 \sin\phi \end{bmatrix}$$

and finally, we design the following control law on the underactuated system (12) using feedback linearization instead of backstepping [27]:

$$\begin{aligned} h = B^{-1}(-Aw - D\dot{C}w + \dot{D}f(z)) \\ + D \frac{\partial f}{\partial z} \dot{z} - k_4(r - Df(z)) \end{aligned} \quad (13)$$

where  $k_4$  is a constant, and

$$\dot{D} = w_2 \begin{bmatrix} -\sin\phi & \cos\phi \\ -\cos\phi/d_0 & \sin\phi/d_0 \end{bmatrix}.$$

In the framework of observer-based controller (10), the inverse calculation the feedback linearization process would aid to obtain the heading angle  $\theta$  furthermore.

### C. Run-Time Optimization

As the size of the robot is much smaller than the scale of the scalar field of concentration, that is a natural hypothesis to suppose  $y(x_1) > y(x_2)$ , and we thus draw an intuitive conclusion that sensor 1 is closer to the source than the sensor 2, which could be further written as an expression as follows:

$$\begin{aligned} \|x - x_1\|^2 \leq \|x - x_2\|^2 \Leftrightarrow \\ \|x - x_r - l_0\|^2 \leq \|x - x_r + l_0\|^2 \end{aligned} \quad (14)$$

so, we could get a general form

$$l_0(x - x_r) \geq 0 \quad (15)$$

in summary of both cases of  $y(x_1) \geq y(x_2)$  and  $y(x_1) < y(x_2)$ , (15) is generalized to be

$$\text{sign}(y(x_1) - y(x_2))l_0(x - x_r) \geq 0 \quad (16)$$

it could be expressed as a set constraint equivalent for  $x \in \mathbb{R}^2$

$$\{x \in \Omega | \text{sign}(y(x_1) - y(x_2))l_0(x - x_r) \geq 0\}. \quad (17)$$

So far we have arrived at two constraints of  $x$ , which includes the equality constraint  $\dot{x} = g(x)$  and the inequality

constraint  $x \in \Omega$ . We thus establish the following filter [29] to improve the estimation

$$\dot{\hat{x}} = g(\hat{x}) - k \frac{\hat{x} - P_\Omega(\hat{x})}{\|\hat{x} - P_\Omega(\hat{x})\|}. \quad (18)$$

As to the  $P_\Omega(\hat{x})$ , it could be obtained as the solution to the following optimization problem [30]

$$\min \|\hat{x} - P_\Omega(\hat{x})\|^2 \quad (19a)$$

$$\text{s.t. } \text{sign}(y(x_1) - y(x_2))l_0(P_\Omega(\hat{x}) - x_r) \geq 0. \quad (19b)$$

Finally, we obtain [31]

$$P_\Omega(\hat{x}) = \begin{cases} \hat{x}, & \text{sign}(y(x_1) - y(x_2))l_0^\top(\hat{x} - x_r) \geq 0 \\ \hat{x} - l_0 l_0^\top(\hat{x} - x_r)/\|l_0\|^2, & \text{otherwise.} \end{cases} \quad (20)$$

## IV. THEORETICAL ANALYSIS

The theoretical analysis is conducted on the stability of the optimization and the convergence of the entire closed-loop control in the section via corresponding theorem.

### A. Stability of the Optimization

In this section, stability theorem is utilized to investigate the performance of the proposed optimization (18).

*Theorem 1:* The optimization (18) is stable and also asymptotically converges to the equilibrium point  $x$ , of which two parts of the projection (20) constitute the bounded area of feedback to optimize the constraint problem (19).

*Proof:* At first, we choose the following Lyapunov function candidate [32], [33]:

$$V = (x - P_\Omega(\hat{x}))^\top(x - P_\Omega(\hat{x}))/2 \quad (21)$$

and then, calculating the derivative of  $V$  according to the optimization (18), we could obtain

$$\begin{aligned} \dot{V} &= (\hat{x} - P_\Omega(\hat{x}))^\top \dot{\hat{x}} \\ &= (\hat{x} - P_\Omega(\hat{x}))g(\hat{x})^\top - k_5\|\hat{x} - P_\Omega(\hat{x})\| \end{aligned} \quad (22)$$

$$\leq \|\hat{x} - P_\Omega(\hat{x})\| \|g(\hat{x})\| - k_5\|\hat{x} - P_\Omega(\hat{x})\| \quad (23)$$

when the coefficient  $k_5$  satisfies  $k_5 > \|g(\hat{x})\|$ ,  $\dot{V} \leq 0$  satisfies, which implies the stability of the proposed optimization and the convergence of  $\hat{x}$  to  $x$ . ■

### B. Convergence of the Closed-Loop Control Structure

*Theorem 2:* The closed-loop control structure [34] incorporating observer-based controller (10) with feedback linearization (13), under Assumptions 1 and 2, handles the source seeking problem mentioned in problem mentioned in the preliminary, i.e., as  $t \rightarrow \infty$  and  $x \rightarrow x_r$ .

*Proof:* There are three steps in the proof including the convergence of the observer (8), the controllers (10), and (13).

*Step 1: The convergence of the observer*

For simplicity, let

$$f(x) = \frac{(v^T \nabla c + k_0 \nabla^2 c) \nabla c}{\|\nabla c\|^2} + \frac{v_d A \nabla c}{\|\nabla c\|} \quad (24)$$

then, the observer (8) could be further reformulated as

$$\dot{\hat{x}} = f(\hat{x}) + k_3 \nabla \hat{x} (c_{\hat{x}} - c_0) \quad (25)$$

the estimation error  $\dot{e} = \mathbf{x} - \hat{\mathbf{x}}$  generates the following dynamic equation:

$$\dot{e} = f(\mathbf{x}) - f(\hat{\mathbf{x}}) + k_3 \nabla \hat{x} (c_{\hat{x}} - c_0). \quad (26)$$

Considering the following first-order approximations:

$$\begin{aligned} c_{\hat{x}} - c_0 &\approx -\nabla^T c (\mathbf{x} - \hat{\mathbf{x}}) = -\nabla^T e, \\ f(\mathbf{x}) - f(\hat{\mathbf{x}}) &\approx \frac{\partial f(\mathbf{x})}{\partial \mathbf{x}} e \end{aligned}$$

the variant of (26) becomes

$$\dot{e} = \left( \frac{\partial f(\mathbf{x})}{\partial \mathbf{x}} - k_3 \nabla c \nabla^T c \right) e. \quad (27)$$

According to the dynamic system of (25) and (27), we could find that  $\mathbf{x}$  evolves much faster than  $e$  in the sense of that the averaging principle applies to (27). Then, we could get

$$\dot{e} \approx \frac{\int_t^{t+T} \left( \frac{\partial f(\mathbf{x})}{\partial \mathbf{x}} - k_6 \nabla c \nabla^T c \right) dt}{T} e = H(\mathbf{x}) e \quad (28)$$

where  $T$  denotes the averaging period and  $H(\mathbf{x})$  is a symmetric matrix satisfying

$$H(\mathbf{x}) = \frac{\int_t^{t+T} \frac{\partial f(\mathbf{x})}{\partial \mathbf{x}}}{T} - k_6 \frac{\int_t^{t+T} \nabla c \nabla^T c}{T}$$

As both  $\nabla c$  and  $\partial f(\mathbf{x})/\partial \mathbf{x}$  are absolute values, it is expected that the symmetric matrix  $H(\mathbf{x})$  of (28) is negative definite, which guarantees the convergence of  $e$  by selecting  $V = e^T e$  as the Lyapunov candidate function, when the coefficient  $k_6$  is large enough [35].

#### Step 2: Convergence of the observer-based controller

Substituting the observer (9) into (10) could generate

$$\dot{x}_r = -k_7(x_r - \hat{x}) + \dot{\hat{x}} \quad (29)$$

hence, the control error  $e' = \hat{x} - x_r$  could be formulated as  $\dot{e}' = -k_7 e'$ , which illustrates the stability of  $e'$  at equilibrium point zero, i.e., as  $t \rightarrow \infty$  and  $\hat{x} \rightarrow x_r$  achieves. According to step 2, the convergence of the observer (9)  $e = \mathbf{x} - \hat{\mathbf{x}} \rightarrow 0$ . Thus,  $\mathbf{x} - x_r = e + e'$  reaches convergence to zero [36], in other words,  $x_r$  converges to  $\mathbf{x}$ .

#### Step 3: Convergence of Feedback Linearization

Given the definition of the velocity error  $e'' = v - f(z)$  and notice that

$$\frac{Df(z)}{dt} = \dot{D}f(z) + D \frac{\partial f}{\partial z} v, CD = I.$$

Based on (12) and (13), we obtain  $\dot{e}'' = -k_7 e''$ , which suffices the convergence of  $e''$  to zero in the sense of that  $v$  converges to  $f(z)$ . In other words, single integrator control for the dynamic model is asymptotically achieved. Evidently,  $\dot{z} = f(z)$  converges much faster as  $k_7$  is larger [37]. ■

## V. ILLUSTRATIVE EXAMPLES

In this section, we present both simulation and robot experiment to validate the efficacy of the proposed algorithm and theorems, whose implementation and responding results are described in the following Sections V-A and V-B.

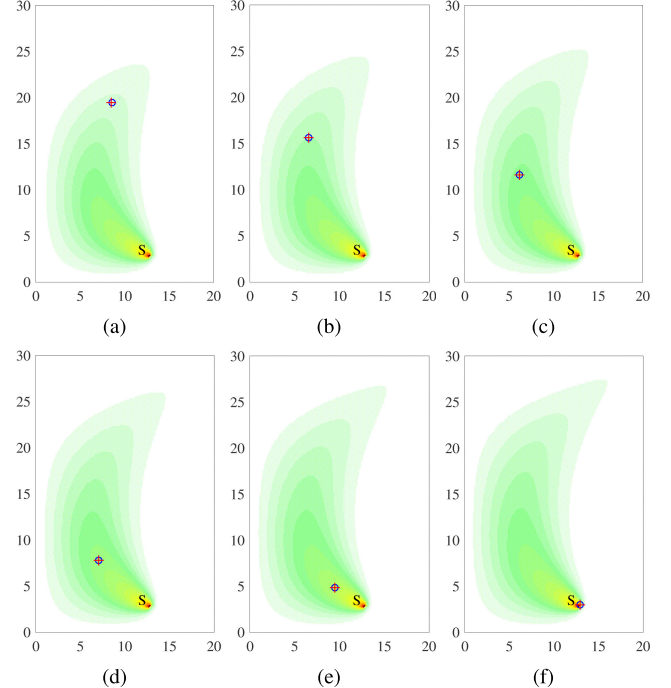


Fig. 3. Snapshots of the robot movements for a typical simulation run with a robot initialized from the point (22 and 12) for source seeking when the concentration difference between the two sensors on the both sides of the robot is measurable and bounded  $l_0 = 0.4$  away from the mass point, the position marked with  $S$  is the source point with the most highest concentration  $c_s = 3$  starting propagating chemicals in the flow field at time  $t = 0$ . The hollow circle in blue represents the estimated position of the robot from the observer (25), and the cross in red represents the actual position of the robot which is driven by the whole control strategies consisting of the observer-based controller (10), the attitude control by feedback linearization (13) and the optimization (18). At time (a)  $t = 9.5$  s, (b)  $t = 10$  s, (c)  $t = 10.5$  s, (d)  $t = 11$  s, (e)  $t = 11.5$  s, and (f)  $t = 12$  s.

### A. Simulation

MATLAB simulations are conducted in a concentration field generated by using propagation model (2) driven by a flow field, in which the representative parameters are set to be: the source point's concentration  $c_s = 3$ , the diffusion coefficient  $k_0 = 0.5$ . Due to the advection mechanism under parameter settings from Navier-Stokes equation [16], the contaminant from the source point propagates to a nonsymmetric contour. The robot is released to seek in the field at time  $t = 9$  s after the source starts to propagate at time  $t = 0$  s, whose patrolling speed is set to be  $v_d = 10$  backwards to the source.

#### Case 1: Source Seeking without Noise

Fig. 3 demonstrates the snapshots of the source seeking with a robot released from the initial point P2. After the robot sets off in the field at time  $t = 9$  s and is recorded firstly at time  $t = 9.5$  s shown in Fig. 3(a), it rapidly approaches to the source point, and finally, as shown in Fig. 3(f) at time  $t = 12$  s, the robot reaches the source point with concentration around  $c_s$ . In addition, to display the detailed source seeking progression, all three trajectories of the robot deployed from different initial points are shown in Fig. 4(a), and the corresponding profiles of the mass point and the reference point of the robot are illustrated in Fig. 4(b) and (c), respectively. It is observable from Fig. 4(b) and (c) that, in spite of different initial points

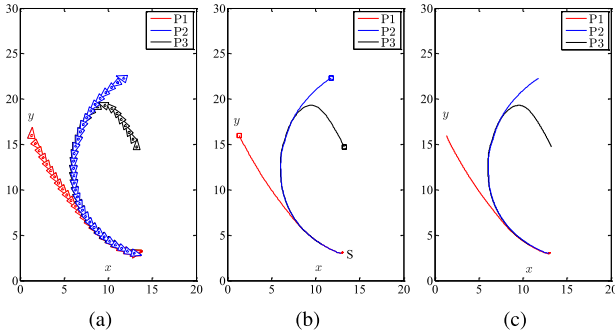


Fig. 4. Trajectories of a robot with different initial points for source tracing in a scalar concentration field, where the solid lines in red, blue, and black correspond to the trajectories started from the initial points such as point 1 (15, 2) (abbreviated as P1), point 2 (22, 12) (abbreviated as P2), and point 3 (15, 12) (abbreviated as P3), respectively. To illustrate the source tracing process clearly, the robot's locations at different initial points and end points shown above are marked in (a)–(c) again to help distinguish different trajectories with initial points. (a) Profiles of the positions along time of the robot from different initial points, where the hollow circle represents the mass point of the robot and the three points of the triangle represent the location of the two sensor, which are  $l_0 = 0.4$  away from the mass point, on the both sides of the robot and the reference point of the robot, respectively. (b) Profiles of the positions along time of the mass point of the robot from different initial points. (c) Profiles of the positions along time of the reference point of the robot from different initial points.

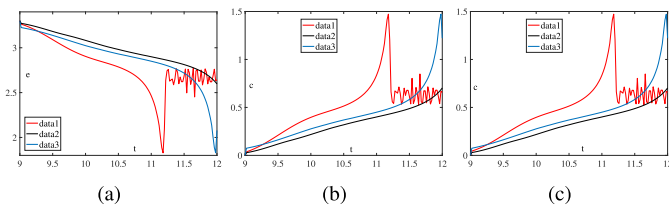


Fig. 5. Performance comparison of the concentration error  $\tilde{e} = c_{x_r} - c_s$  and time profiles of concentration along the time histories with different initial points such as point 1 (15, 2) (abbreviated as P1), point 2 (22, 12) (abbreviated as P2), and point 3 (15, 12) (abbreviated as P3), respectively. (a) Concentration error  $\tilde{e}$  between the concentration measurement and the concentration threshold at source point relative to three different initial points. (b) Time profile of the concentration denoting the concentration measurement at the position where the robot reaches by the control-based source seeking strategy relative to three different initial points. (c) Time profile of the concentration denoting the concentration at the position estimated with the observer (25) relative to three different initial points.

for the all three kinds of trajectories, all of them achieve the source seeking tasks successfully. Results in aforementioned simulations justify the effectiveness of the control structure consisting of (10) and (13) and substantiate the efficacy of the stability of the closed-loop system in theorem 1.

The concentration results corresponding to the three trajectories initialized from three different points are shown in Fig. 5 in detail. Specifically speaking, Fig. 5(a) plots that trajectories of the errors between realtime concentration measurement and the concentration of the source point with different initial points converge to low level as the robot approach to the source point. Besides, Fig. 5(b) and (c) demonstrates the concentration profiles at the actual position  $x_r$  and the estimated position  $\hat{x}$  of the mass point of the robot, respectively, which validate the efficacy of the proposed optimization algorithm (18) and the stability proved in theorem 1.

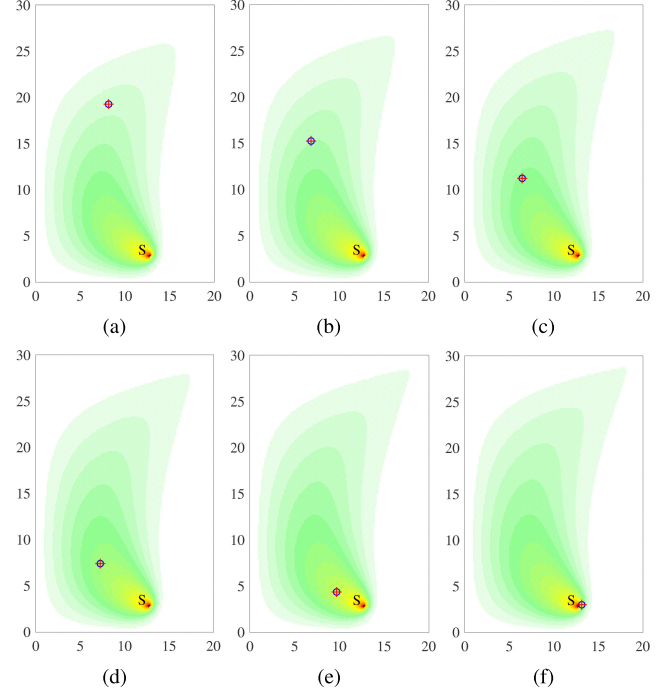


Fig. 6. Snapshots of the robot movements for a typical simulation run with a robot initialized from the point (24, 13) for source seeking when the concentration difference between the two sensors on the both sides of the robot is measurable and  $l_0 = 0.6$  m away from the mass point, in addition, the diffusion coefficient  $k$  of the concentration field is unknown and bounded, the position marked with  $S$  is the source point with the most highest concentration  $c_s = 3$  starting propagating chemicals in the flow field at time  $t = 0$  s  $P$ . The hollow circle in blue represents the estimated position of the robot from the observer (25), and the cross in red represents the actual position of the robot which is driven by the whole control strategies consisting of the observer-based controller (10), the attitude control by feedback linearization (13), and the optimization (18). At time (a)  $t = 9.5$  s, (b)  $t = 10$  s, (c)  $t = 10.5$  s, (d)  $t = 11$  s, (e)  $t = 11.5$  s, and (f)  $t = 12$  s.

### Case 2: Source Seeking with Bounded Parameter

It can be observable from Fig. 6 that, though perturbed by the known bounded parameters and deployed from a farther initial point, the snapshots of the robot seeking source point still converge much faster than that demonstrated in Fig. 3. In addition, Figs. 7 and 8 illustrate the trajectories of source seeking and the corresponding concentration profiles, which substantiate the superiority of the proposed strategy consisting of (10), (13), and (18) and the efficacy of Theorems 1 and 2.

### B. Experiment

In this section, the proposed control algorithm is tested by using a car-like robot to explore an odor source in an alcohol field driven by wind, which could justify the proposed source seeking method effectively by considering actual conditions.

The test bed is built on a  $4 \text{ m} \times 4 \text{ m}$  area covered by pieces of white boards. We place the odor source on the floor in order to imitate the situation of contaminant spill in scalar field. Robot used in experiments is a differential-drive robot modified from the 4WD-skeletonbot controlled by Arduino. The robot is equipped with an alcohol measuring module to measure the concentration of the alcohol in real time. Fig. 9(a) is a photograph of the robot. Fig. 9(b) illustrates the experiment environment with both alcohol source and the fan in which experiments were conducted.

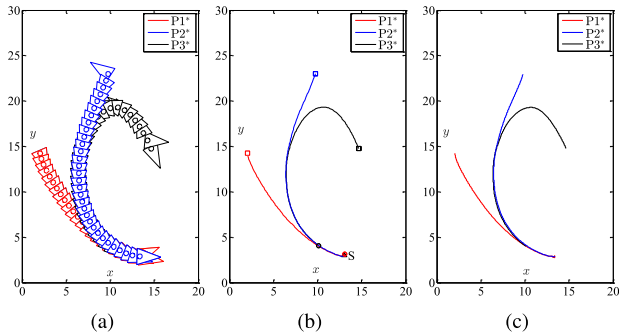


Fig. 7. Trajectories of a robot with different initial points for source tracing in a scalar concentration field with unknown diffusion coefficient  $k_0$ , where the solid lines in red, blue, and black correspond to the trajectories started from the initial points point 1\* (15, 1) (abbreviated as P1\*), point 2\* (24, 13) (abbreviated as P2\*), and point 3\* (15, 14) (abbreviated as P3\*), respectively. To illustrate the source tracing process clearly, the robot's locations with different initial points and end points shown above are marked in (a)–(c) again to help distinguish different trajectories with initial points. (a) Profiles of the positions along time of the robot from different initial points, where the hollow circle represents the mass point of the robot and the three points of the triangle represent the location of the two sensor, which are  $l_0 = 0.6$  away from the mass point, on the both sides of the robot and the reference point of the robot, respectively. (b) Profiles of the positions along time of the mass point of the robot from different initial points. (c) Profiles of the positions along time of the reference point of the robot from different initial points.

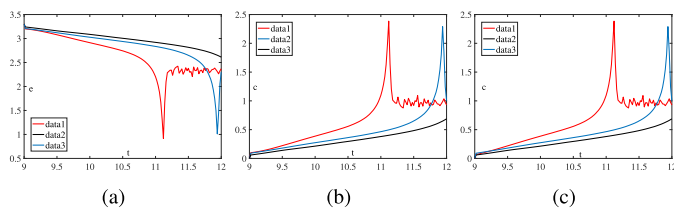


Fig. 8. Performance comparison of the concentration error  $\tilde{e} = c_{x_r} - c_s$  and time profiles of concentration along the time histories with different initial points such as point 1\* (15, 1) (abbreviated as P1\*), point 2\* (24, 13) (abbreviated as P2\*), and point 3\* (15, 14) (abbreviated as P3\*), respectively. The concentration scalar field suffers from the unknown coefficient  $k$ . (a) Concentration error  $\tilde{e}$  between the concentration measurement and the concentration threshold at source point relative to three different initial points. (b) Time profile of the concentration denoting the concentration measurement at the position where the robot reaches by the control-based source seeking strategy relative to three different initial points. (c) Time profile of the concentration denoting the concentration at the position estimated with the observer (25) relative to three different initial points.

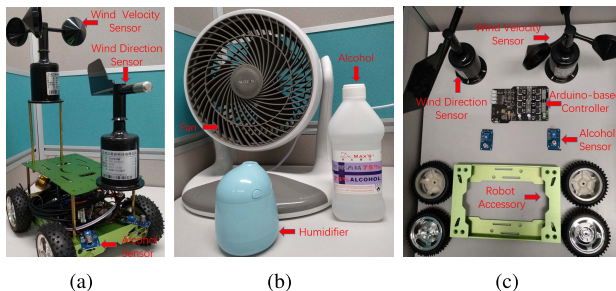


Fig. 9. Robot and alcohol source for source seeking. (a) 4WD-Skeletonbot robot equipped with wind sensor and alcohol sensor. (b) Source point constructed with a fan and a humidifier for source seeking. (c) Disassembled parts of the experimental system.

Fig. 9(c) demonstrates the accessories and sensors of the platform. The 4WD-skeletonbot robot is deployed in the alcohol field, whose initial relative positions are randomly chosen as  $(0.7, 0.4)$  and  $(3.4, 0.7)$  with bearings 0 and 0, respectively.

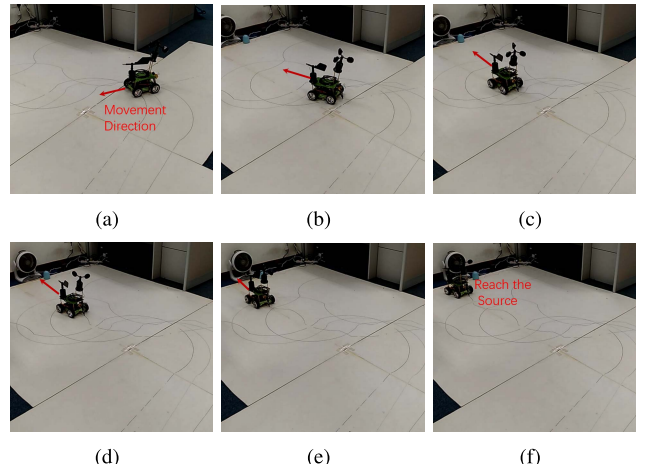


Fig. 10. Alcohol source seeking with the 4WD-skeletonbot in an indoor environment. (a) At  $t = 2$  s time instance at point(2.9,0.9). (b) At  $t = 4$  s time instance at point (2,1). (c) At  $t = 6$  s time instance at point (1.8,1.5). (d) At  $t = 8$  s time instance at point (1.5,2). (e) At  $t = 10$  s time instance at point (1.2,2.5). (f) At  $t = 12$  s time instance at point (1.6,3.3).

TABLE I  
POSITION RECORDS CONSIDERING TWO DIFFERENT  
INITIAL POINTS FROM SAMPLING TIME  $t_1-t_6$

	$t_1(2s)$	$t_2(4s)$	$t_3(6s)$	$t_4(8s)$	$t_5(10s)$	$t_6(12s)$
$P_A$	1.0465	1.4825	1.7441	2.1802	2.6162	3.0000
	2.1333	1.7500	1.4333	1.5000	1.2333	1.2000
$P_B$	0.6976	1.1337	1.5174	1.6046	2.0058	2.9651
	2.4666	2.9166	2.5333	1.2000	0.7333	1.1666

Fig. 10 displays the snapshots of alcohol source exploration in the indoor experiment environment using a robot, which set off from the initial point (3.4, 0.7), which demonstrates the convergence of the robot to the alcohol source and substantiates the proposed control structure.

As demonstrated in Table I, the initial positions are randomly chosen as (3.4, 0.7) named as  $P_A$  and (0.7, 0.4) named as  $P_B$ , respectively, and the sampling times are at 6 time instances, i.e.,  $t_1 = 2$  s,  $t_2 = 4$  s,  $t_3 = 6$  s,  $t_4 = 8$  s,  $t_5 = 10$  s, and  $t_6 = 12$  s. The trajectories of the robot setting off from both  $P_A$  and  $P_B$  could be regenerated according to the sampling points as shown in Table I. Though the initial positions are randomly chosen, the robot moves toward the source point all the way. It can be observed from the above analysis that the proposed source seeking strategy guarantees the robustness and achieves stability in the practical application.

## VI. CONCLUSION

We consider the control structure for source seeking using a robot. two controllers incorporate into a closed loop structure on both kinematic and dynamic levels by accompanying with a bio-inspired optimization algorithm.

## REFERENCES

- [1] M. Hutchinson, H. Oh, and W. H. Chen, "A review of source term estimation methods for atmospheric dispersion events using static or mobile sensors," *Inf. Fusion*, vol. 36, pp. 130–148, Jul. 2017.
  - [2] W. He, Z. Yin, and C. Sun, "Adaptive neural network control of a marine vessel with constraints using the asymmetric barrier Lyapunov function," *IEEE Trans. Cybern.*, vol. 47, no. 7, pp. 1641–1651, Jul. 2017.

- [3] W. He, X. Mu, Y. Chen, X. He, and Y. Yu, "Modeling and vibration control of the flapping-wing robotic aircraft with output constraint," *J. Sound Vibrat.*, vol. 423, pp. 472–483, Jun. 2018.
- [4] R. A. Russell, A. Bab-Hadiashar, and R. L. Shepherd, "A comparison of reactive robot chemotaxis algorithms," *Robot. Auto. Syst.*, vol. 45, no. 2, pp. 83–97, 2003.
- [5] M. Vergassola, E. Villermaux, B. I. Shraiman, "‘Infotaxis’ as a strategy for searching without gradients," *Nature*, vol. 445, no. 7126, pp. 406–409, 2007.
- [6] J. Masson, M. B. Bechet, and M. Vergassola, "Chasing information to search in random environments," *J. Phys. A Math. Theor.*, vol. 42, no. 43, pp. 434009–434014, 2016.
- [7] H. Hajieghrary, M. A. Hsieh, and I. B. Schwartz, "Multi-agent search for source localization in a turbulent medium," *Phys. Lett. A*, vol. 380, no. 20, pp. 1698–1705, 2016.
- [8] R. Zou, V. Kalivarapu, and E. Winer, "Particle swarm optimization-based source seeking," *IEEE Trans. Autom. Sci. Eng.*, vol. 12, no. 3, pp. 865–875, Jul. 2015.
- [9] S. Pang and J. A. Farrell, "Chemical plume source localization," *IEEE Trans. Syst., Man, Cybern. B, Cybern.*, vol. 36, no. 5, pp. 1068–1080, Oct. 2006.
- [10] J. G. Li, Q. H. Meng, and Y. Wang, "Odor source localization using a mobile robot in outdoor airflow environments with a particle filter algorithm," *Auton. Robots*, vol. 30, no. 3, pp. 281–292, 2011.
- [11] J. Cochran, E. Kanso, S. D. Kelly, H. Xiong, and M. Krstic, "Source seeking for two nonholonomic models of fish locomotion," *IEEE Trans. Robot.*, vol. 25, no. 5, pp. 1166–1176, Oct. 2009.
- [12] J. Cochran, A. Siranosian, N. Ghods, and M. Krstic, "3-D source seeking for underactuated vehicles without position measurement," *IEEE Trans. Robot.*, vol. 25, no. 1, pp. 117–129, Feb. 2009.
- [13] L. Fu and U. Ozguner, "Extremum-seeking control in constrained source tracing with nonholonomic vehicles," *IEEE Trans. Ind. Electron.*, vol. 56, no. 9, pp. 3602–3608, Sep. 2009.
- [14] A. Raisch and M. Krstic, "Overshoot-free steering-based source seeking," *IEEE Trans. Control Syst. Technol.*, vol. 25, no. 3, pp. 818–827, May 2017.
- [15] S. Li, R. Kong, and Y. Guo, "Cooperative distributed source seeking by multiple robots: Algorithms and experiments," *IEEE/ASME Trans. Mechatronics*, vol. 19, no. 6, pp. 1810–1820, Dec. 2014.
- [16] S. Li, Y. Guo, and B. Bingham, "Multi-robot cooperative control for monitoring and tracking dynamic plumes," in *Proc. IEEE Int. Conf. Robot. Autom. (ICRA)*, Jun. 2014, pp. 67–73.
- [17] Y. Zhang, S. Chen, S. Li, and Z. Zhang, "Adaptive projection neural network for kinematic control of redundant manipulators with unknown physical parameters," *IEEE Trans. Ind. Electron.*, vol. 65, no. 6, pp. 4909–4920, Jun. 2017.
- [18] X. Liu, H. Chen, C. Wang, F. Hu, and X. Yang, "MPC control and path planning of Omni-directional mobile robot with potential field method," in *Intell. Robot. Appl.*, 2018, pp. 170–181.
- [19] L. Jin and S. Li, "Distributed task allocation of multiple robots: A control perspective," *IEEE Trans. Syst., Man, Cybern. Syst.*, vol. 48, no. 5, pp. 693–701, May 2018.
- [20] W. He, S. Zhang, and S. S. Ge, "Robust adaptive control of a thruster assisted position mooring system," *Automatica*, vol. 50, no. 7, pp. 1843–1851, 2014.
- [21] Q. Hu, Q. Hu, C. Du, L. Xie, and Y. Wang, "Discrete-time sliding mode control with time-varying surface for hard disk drives," *IEEE Trans. Control Syst. Technol.*, vol. 17, no. 1, pp. 175–183, Jan. 2009.
- [22] K. You and L. Xie, "Kalman filtering with scheduled measurements," *IEEE Trans. Signal Process.*, vol. 61, no. 6, pp. 1520–1530, Mar. 2013.
- [23] H. Liu, Y. Pan, S. Li, and Y. Chen, "Adaptive fuzzy backstepping control of fractional-order nonlinear systems," *IEEE Trans. Syst., Man, Cybern. Syst.*, vol. 47, no. 8, pp. 2209–2217, Aug. 2017.
- [24] Y. J. Liu and S. Tong, "Adaptive fuzzy identification and control for a class of nonlinear pure-feedback MIMO systems with unknown dead zones," *IEEE Trans. Fuzzy Syst.*, vol. 23, no. 5, pp. 1387–1398, Oct. 2015.
- [25] C. L. P. Chen, G. X. Wen, Y. J. Liu, and Z. Liu, "Observer-based adaptive backstepping consensus tracking control for high-order nonlinear semi-strict-feedback multiagent systems," *IEEE Trans. Cybern.*, vol. 46, no. 7, pp. 1591–1601, Jul. 2016.
- [26] X. Jiang and S. Li, "Plume front tracking in unknown environments by estimation and control," *IEEE Trans. Ind. Informat.*, vol. 15, no. 2, pp. 911–921, Feb. 2019. doi: [10.1109/TII.2018.2831225](https://doi.org/10.1109/TII.2018.2831225).
- [27] B. Xu, Z. Shi, C. Yang, and F. Sun, "Composite neural dynamic surface control of a class of uncertain nonlinear systems in strict-feedback form," *IEEE Trans. Cybern.*, vol. 44, no. 12, pp. 2626–2634, Dec. 2014.
- [28] R. Olfati-Saber, "Normal forms for underactuated mechanical systems with symmetry," *IEEE Trans. Autom. Control*, vol. 47, no. 2, pp. 305–308, Feb. 2002.
- [29] D. Han, K. You, L. Xie, J. Wu, and L. Shi, "Optimal parameter estimation under controlled communication over sensor networks," *IEEE Trans. Signal Process.*, vol. 63, no. 24, pp. 6473–6485, Dec. 2015.
- [30] K. You, L. Xie, and S. Song, "Asymptotically optimal parameter estimation with scheduled measurements," *IEEE Trans. Signal Process.*, vol. 61, no. 14, pp. 3521–3531, Jul. 2013.
- [31] H. Wang, H. R. Karimi, P. X. Liu, and H. Yang, "Adaptive neural control of nonlinear systems with unknown control directions and input dead-zone," *IEEE Trans. Syst., Man, Cybern. Syst.*, vol. 48, no. 11, pp. 1897–1907, Nov. 2018. doi: [10.1109/TSMC.2017.2709813](https://doi.org/10.1109/TSMC.2017.2709813).
- [32] X. Li and J. Wu, "Sufficient stability conditions of nonlinear differential systems under impulsive control with state-dependent delay," *IEEE Trans. Autom. Control*, vol. 63, no. 1, pp. 306–311, Jan. 2016.
- [33] S. Li, M. Zhou, and X. Luo, "Modified primal-dual neural networks for motion control of redundant manipulators with dynamic rejection of harmonic noises," *IEEE Trans. Neural Netw. Learn. Syst.*, vol. 29, no. 10, pp. 4791–4801, Oct. 2018.
- [34] W. He, Z. C. Yan, C. Y. Sun, and Y. Chen, "Adaptive neural network control of a flapping wing micro aerial vehicle with disturbance observer," *IEEE Trans. Cybern.*, vol. 47, no. 10, pp. 3452–3465, Oct. 2017.
- [35] X. Li and S. Song, "Stabilization of delay systems: Delay-dependent impulsive control," *IEEE Trans. Autom. Control*, vol. 62, no. 1, pp. 406–411, Jan. 2017.
- [36] D. Chen, Y. Zhang, and S. Li, "Tracking control of robot manipulators with unknown models: A jacobian-matrix-adaption method," *IEEE Trans. Ind. Informat.*, vol. 14, no. 7, pp. 3044–3053, Jul. 2018.
- [37] B. Xu, C. Yang, and Y. Pan, "Global neural dynamic surface tracking control of strict-feedback systems with application to hypersonic flight vehicle," *IEEE Trans. Neural Netw. Learn. Syst.*, vol. 26, no. 10, pp. 2563–2575, Oct. 2015.